The Astrophysical Journal, 969:3 (11pp), 2024 July 1 https://doi.org/10.3847/1538-4357/ad4640

Electron Cyclotron Maser Emission and the Brightest Solar Radio Bursts

Stephen M. White[1,2], Masumi Shimojo[3], Kazumasa Iwai[4], Timothy S. Bastian[5], Gregory D. Fleishman[6,7], Dale E. Gary[6], Jasmina Magdalenic[8,9], and Angelos Vourlidas[10]
[1] Space Vehicles Directorate, Air Force Research Laboratory, Kirtland AFB, NM 8711, USA; stephen.white.24@us.af.mil
[2] Department of Physics and Astronomy, University of New Mexico, Albuquerque, NM 87106, USA
[3] National Astronomical Observatory of Japan, Mitaka, Tokyo 181-8588, Japan
[4] Institute for Space-Earth Environmental Research, Nagoya University, Nagoya 464-8601, Japan
[5] National Radio Astronomy Observatory, Charlottesville, VA 22903-2475, USA
[6] Center for Solar-Terrestrial Research, New Jersey Institute of Technology, Newark, NJ 07102, USA
[7] Institut für Sonnenphysik (KIS), Schöneckstrasse 6, D-79104 Freiburg, Germany
[8] Solar-Terrestrial Centre of Excellence- SIDC, Royal Observatory of Belgium, 1180 Uccle, Belgium
[9] Centre for Mathematical Plasma Astrophysics, Department of Mathematics, KU Leuven, B-3001 Leuven, Belgium
[10] The Johns Hopkins University Applied Physics Laboratory, 11100 Johns Hopkins Road, Laurel, MD 20723-6099, USA
Received 2024 March 5; revised 2024 April 22; accepted 2024 April 22; published 2024 June 21

Abstract

This paper investigates the incidence of coherent emission in solar radio bursts, using a revised catalog of 3800 solar radio bursts observed by the Nobeyama Radio Polarimeters from 1988 to 2023. We focus on the 1.0 and 2.0 GHz data, where radio fluxes of order 10^{10} Jy have been observed. Previous work has suggested that these bursts are due to electron cyclotron maser (ECM) emission. In at least one well-studied case, the bright emission at 1 GHz consists of narrowband spikes of millisecond duration. Coherent emission at 1 GHz can be distinguished from traditional incoherent gyrosynchrotron flare emission based on the radio spectrum: Gyrosynchrotron emission at 1 GHz usually has a spectrum rising with frequency, so bursts in which 1 GHz is stronger than higher-frequency measurements are unlikely to be incoherent gyrosynchrotron. Based on this criterion, it is found that for bursts exceeding 100 sfu, three-quarters of all bursts at 1 GHz and half of all 2 GHz bursts have a dominant coherent emission component, assumed to be ECM. The majority of the very bright bursts at 1 GHz are highly circularly polarized, consistent with a coherent emission mechanism, but not always 100% polarized. The frequency range from 1 to 2 GHz is heavily utilized for terrestrial applications, and these results are relevant for understanding the extreme flux levels that may impact such applications. Further, they provide a reference for comparison with the study of ECM emission from other stars and potentially exoplanets.

Unified Astronomy Thesaurus concepts: Solar flares (1496); Solar activity (1475); Solar radio emission (1522); Solar radio flares (1342)

Supporting material: figure set

1. Introduction

Of the five mechanisms known to contribute to the radio emission of the Sun, electron cyclotron maser (ECM) emission is the least well studied in terms of occurrence and association with other solar phenomena. The other mechanisms (thermal bremsstrahlung, thermal gyroresonance, nonthermal gyrosynchrotron, and nonthermal plasma emission) are well known and their roles in the different aspects of solar radio emission are fairly well understood (see, e.g., the review articles in Gary & Keller 2004).

Although there had been considerable interest in applications of maser forms of cyclotron emission to astrophysics previously (e.g., Melrose 1976, and references therein), modern interest was reinvigorated when Wu & Lee (1979) pointed out that the inclusion of semi-relativistic effects in the cyclotron resonance condition enables strong maser action for a much wider and more plausible range of electron velocity distributions than was previously thought. In particular, loss-cone velocity distributions, known to be common in planetary radiation belts, were shown to be unstable to maser action, and the ECM mechanism then became plausible as the likely source of terrestrial auroral kilometric radiation (AKR; Wu & Lee 1979; Lee et al. 1980; Melrose et al. 1982) and of Jovian decametric radiation (DAM; e.g., Hewitt et al. 1982), both high-brightness-temperature radio emissions from locally strong magnetic field regions in planetary magnetospheres exhibiting a lot of structure on fine frequency- and temporal-scales. Subsequently, Ergun et al. (2000) showed that a "horseshoe" velocity distribution was more effective for ECM and more likely to be the driver of AKR than the loss-cone distribution.

Holman et al. (1980) and Melrose & Dulk (1982) suggested that certain types of solar radio bursts might also be due to cyclotron maser emission. Dröge (1977) and Slottje (1978) had reported solar radio bursts with narrow bandwidths, durations of the order of milliseconds, and inferred brightness temperatures in excess of 10^{12} K, requiring a coherent emission mechanism. Furthermore, Slottje (1978) showed that the spike bursts could be 100% circularly polarized, which is consistent with the known properties of the cyclotron maser emission. The other potential mechanism for high-brightness-temperature, highly polarized radio bursts is plasma emission, known to be dominant at frequencies below about 300 MHz in the solar corona (e.g., McLean & Labrum 1985). Plasma emission and cyclotron emission each represent the role of the fundamental

physical characteristics of the solar corona, electron density in the case of plasma emission and magnetic field in the case of cyclotron emission. Plasma emission is generated at the fundamental of the electron plasma frequency f_p and its (low) harmonics, where $f_p = 9000\sqrt{n_e}$ (in hertz) depends only on the ambient electron density n_e (per cubic centimeter). Plasma emission at the fundamental frequency f_p can be 100% polarized in the sense of the O mode. Cyclotron maser emission occurs at the electron-cyclotron frequency, $\Omega_B = 2.8 \times 10^6 B$ (Hz), and its harmonics, where B is the magnetic field strength (in gauss); generally, cyclotron maser emission is expected to be polarized in the sense of the X mode. There has been extensive discussion of whether plasma emission or cyclotron maser emission is responsible for solar spike bursts (e.g., Fleishman & Mel'nikov 1998; Chernov 2011; Cliver et al. 2022), which we will not rehash here. We note that Guedel & Zlobec (1991) found that when spike bursts occur in conjunction with Type III bursts, the spike bursts always had the opposite polarization. Since Type III bursts are known to be plasma emission and therefore likely to be O-mode polarized, this implies that the spikes were in the X mode, which is an argument in favor of ECM. Similarly, Fleishman et al. (2003) found that spike polarization matched that of the associated higher-frequency, optically thin gyrosynchrotron emission, indicating X-mode polarization. Since free–free absorption varies roughly as $n_e^2\, T^{-0.5}$, where T is the ambient temperature, and $f_p \propto n_e^{0.5}$, the absorption of fundamental plasma emission increases as a high power of emission frequency, and this is believed to explain its relative rarity at GHz frequencies (although it may be more likely in high-temperature environments; e.g., White & Franciosini 1995). Solar spike bursts have been seen at least up to 8 GHz (Benz et al. 1992).

In this paper, we adopt the assumption that high-brightness-temperature, highly polarized bursts at around 1 GHz are due to cyclotron maser emission. We describe a prototype example in the next section. Our focus in this paper is not on spike bursts themselves, but rather on the occurrence of solar radio bursts with these properties. One of our prime motivations is the fact that such bursts can produce perhaps the most intense natural radio emission observable from the Earth's surface (of order 10^{-16} W m^{-2} Hz^{-1}; e.g., Gary 2019; Gary & Bastian 2021; Cliver et al. 2022), and can dramatically affect the operation of global navigation satellite systems such as the Global Positioning System (GPS; see, e.g., Cerruti et al. 2008; Carrano et al. 2009). A better understanding of such bursts can help to identify the physical conditions under which they arise and has implications for space-weather impacts. Another important consideration is the increasing interest in cyclotron maser emission (analogous to AKR) associated with particles trapped in magnetospheres around stars such as brown dwarfs (Hallinan et al. 2006) and magnetic B stars (Trigilio et al. 2000). Such stars exhibit pulsed radio emission, presumably due to the rotation of the stars, and the radio emission provides an important diagnostic of magnetic field properties and other features of these systems. A better understanding of the occurrence of ECM on the Sun may inform broader astrophysical applications. To this end, in this paper we survey the solar radio burst measurements by the Nobeyama Radio Polarimeters (NoRP; Nakajima et al. 1985; Shimojo & Iwai 2023, and references therein) at 1.0, 2.0, and 3.75 GHz since 1988. These data are available daily during Japanese daylight hours for essentially the whole period, and importantly provide circular polarization measurements absent in other comparable data sets. We show from spectral considerations that ECM is, in fact, surprisingly common in solar radio bursts at 1 GHz, and that bright ECM emission lasting for an hour or more is not unusual in intense bursts at this frequency.

2. Solar Radio Burst of 2006 December 6

The poster child for bright L-band solar radio bursts is the 2006 December 6 X9.3 flare, because it was well observed by several radio instruments.[11] This event, along with several other bright bursts from the same active region, has been discussed by Gary (2019) and Nita et al. (2014). Radio emission reached a peak flux of order 10^6 sfu at 1.4 GHz, at which level it rendered civilian GPS receivers in the Western Hemisphere largely unusable for about 20 minutes (Cerruti et al. 2008; Carrano et al. 2009).[12] The brightest emission in the 1.0–1.5 GHz range occurred some 45 minutes after the peak of the soft X-ray (SXR) flare. Strong but rapidly fluctuating emission was seen at least across the full frequency range from 1.0 to 1.5 GHz, with orders-of-magnitude variation seen on timescales of minutes.

One of the instruments that observed the flare was the FASR Subsystem Testbed (FST) at Owens Valley Radio Observatory (OVRO; Liu et al. 2007), which sampled the 1.0–1.5 GHz frequency range at the (then) very high data rate of 1 Gsps.[13] The system alternated right-circular (RCP) and left-circular (LCP) polarizations on a 4 s timescale. Due to limitations in the speed of writing data to disk at the time, data were acquired for 100 μs, then the system waited 20 ms while the data were written out. Thus, timescales between 0.1 and 20 ms were not measured. Three antennas were recorded simultaneously for use as an interferometer. The recorded time-domain data were Fourier sampled to 512 frequency channels, effectively each 1 MHz wide, and accumulated over 97 μs to form each snapshot spectrum. Figure 1 shows the result of stacking these spectra in time for several consecutive 4 s intervals in RCP, where the structure of the burst can be seen. Intense spikes several MHz wide and shorter than the effective time resolution of 20 ms are seen across the entire spectrum, with a higher density towards the lower end of the frequency range. Other forms of emission are present, but the flux is dominated by the spikes, which are close to 100% RCP. No temporal structure is seen in individual spikes within the fully sampled 100 μs data periods, implying durations significantly longer than 0.1 ms (consistent with the millisecond durations found in the earlier studies; e.g., Dröge 1977; Benz 1986; Benz et al. 1991; Rozhansky et al. 2008; Dąbrowski et al. 2011). No drift in frequency was seen over 100 μs data periods, but that does not mean that it would not be evident over the full duration of a spike.

Figure 1 demonstrates that, when measured at a coarser 1 s time resolution typical of solar radio flux monitors, individual spikes would not be fully resolved; rather, they would appear to form a structured broadband continuum. As noted by Gary (2019), intense events such as this with such high densities of spikes seem qualitatively different from most flares in which spikes are observed for shorter durations at much lower

[11] On the new NOAA "science-quality" scale for GOES soft X-ray flux; X6.5 on the old scale.
[12] 1 solar flux unit (sfu) = 10^4 Jy = 10^{-22} W m^{-2} Hz^{-1}.
[13] Giga (10^9) samples per second.

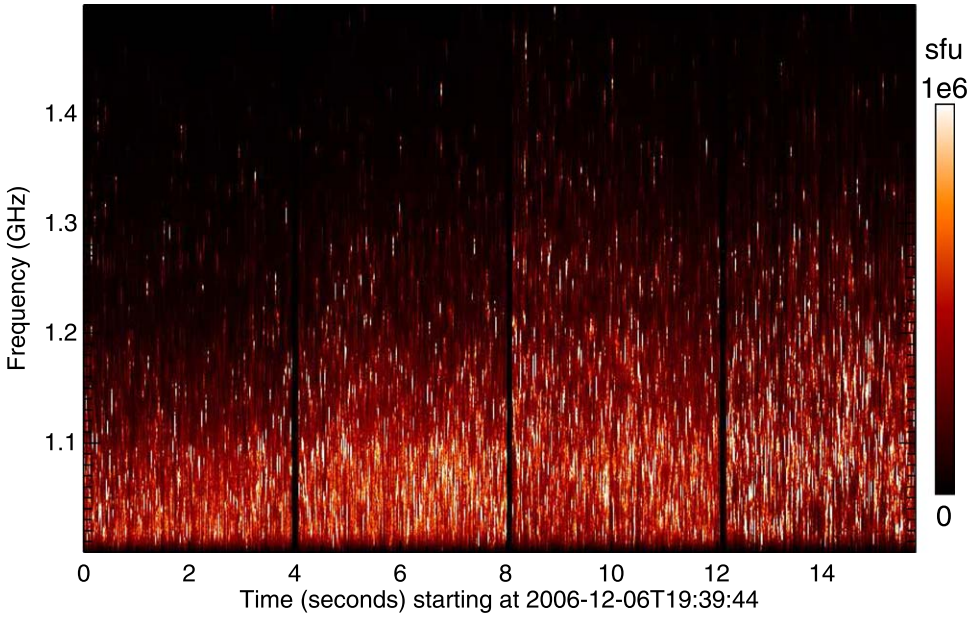

Figure 1. A plot of 15 s of RCP FST data sampling the correlated amplitude on a single baseline around the time of the peak at 1.4 GHz from the flare on 2006 December 6. Vertical black bars denote gaps in real time of 4 s while LCP is being recorded. The frequency resolution is 1 MHz. The data consist of 100 μs samples plotted every 20 ms. The flux scale is shown by the color bar at right, (roughly) calibrated against the OVRO flux measurements at 1.2 GHz (see Gary 2019). The brightest spikes shown reach around 5×10^6 sfu averaged over 100 μs; the brightest 1 μs long 1 MHz wide samples reach around 3×10^7 sfu.

densities and with much weaker contributions to the overall flux level. In particular, while spikes are seen up to 8 GHz (e.g., Csillaghy & Benz 1993), extreme flux densities at the levels seen in this event seem to be restricted to frequencies below 3 GHz. Flare radio emission at higher frequencies is dominated by incoherent gyrosynchrotron emission from the nonthermal electrons that also produce flare hard X-rays (HXRs). This has a spectrum that typically increases at low frequencies, where the emission is optically thick, to a peak at around 10 GHz (Nita et al. 2004), and decreases at (the optically thin) frequencies above that peak (e.g., Ramaty 1969; Takakura & Scalise 1970). Thus, a straightforward method to identify events with a potentially significant ECM contribution to the radio flux at, say, 1.0 GHz is to look for bursts in which flux does not increase with frequency as it would with a gyrosynchrotron spectrum. We explore this approach in the following sections.

3. Nobeyama Radio Polarimeter Catalog of Solar Radio Bursts

NoRP (operated by the National Astronomical Observatory of Japan) provides data at 1.0, 2.0, 3.75, 9.4, 17, and 35 GHz at 1 s time resolution in both left- and right-circular polarization.[14,15] As noted above, strong circular polarization is often a characteristic of ECM emission, and we are interested in determining how often high degrees of polarization are seen in bursts, so NoRP provides the best data source for such a study. In addition, the NoRP data do not suffer from artificial limits on flux reporting and occasional saturation that has affected Radio Solar Telescope Network (RSTN) data at times (see discussion of this issue for RSTN data in Giersch et al. 2017). A catalog of NoRP solar radio bursts from 1988 is provided online (used by Song et al. 2012, for their study of NoRP burst flux distributions), but it ceased to be maintained after early 2015 due to resource issues.[16] Further, inclusion of radio bursts did not occur in an organized fashion in the early years, so there are missing bursts that would likely have been recorded in more recent years. Since we wish to have as complete a survey of ECM bursts as possible, we have therefore generated a new catalog of NoRP bursts from 1988 to 2023 using a combination of automated detection and manual verification (also used for a statistical study of "cold" solar flares; Lysenko et al. 2023).[17] The new catalog should be reasonably complete for bursts with flux exceeding 50 sfu in the 1–17 GHz range; it contains 3818 events, compared to 856 events in the previous catalog. Note that this is a radio-selected catalog of bursts, not flare selected, so flares in which multiple bursts occurred well separated in time, particularly at 1.0 GHz, may be represented more than once (e.g., the flare of 2006 December 13 discussed further below). Shimojo & Iwai (2023) describe the history of the NoRP data and issues at each frequency over the years that can result in spurious features, and we have tried to take these into account in the analysis. Generally, a clear burst detection at more than one frequency was required for the burst to be included in the list. However, bursts are included at 1.0 and 2.0 GHz in the absence of higher-frequency emission if they are associated with a clear prior event; the results of this paper will justify that approach.

4. Survey of Electron Cyclotron Maser in Solar Radio Bursts

We focus on using the burst emission at the three lowest NoRP frequencies since the brightest ECM bursts so far have occurred at frequencies below 2 GHz. For an initial survey, in Figure 2 we plot the degree of polarization versus peak flux at each frequency for all bursts where the flux at that frequency

[14] NoRP data at 0.1 s time resolution is also available for bright bursts.
[15] See http://solar.nro.nao.ac.jp/norp/index.html.
[16] See http://solar.nro.nao.ac.jp/norp/html/event/.
[17] By S.W.

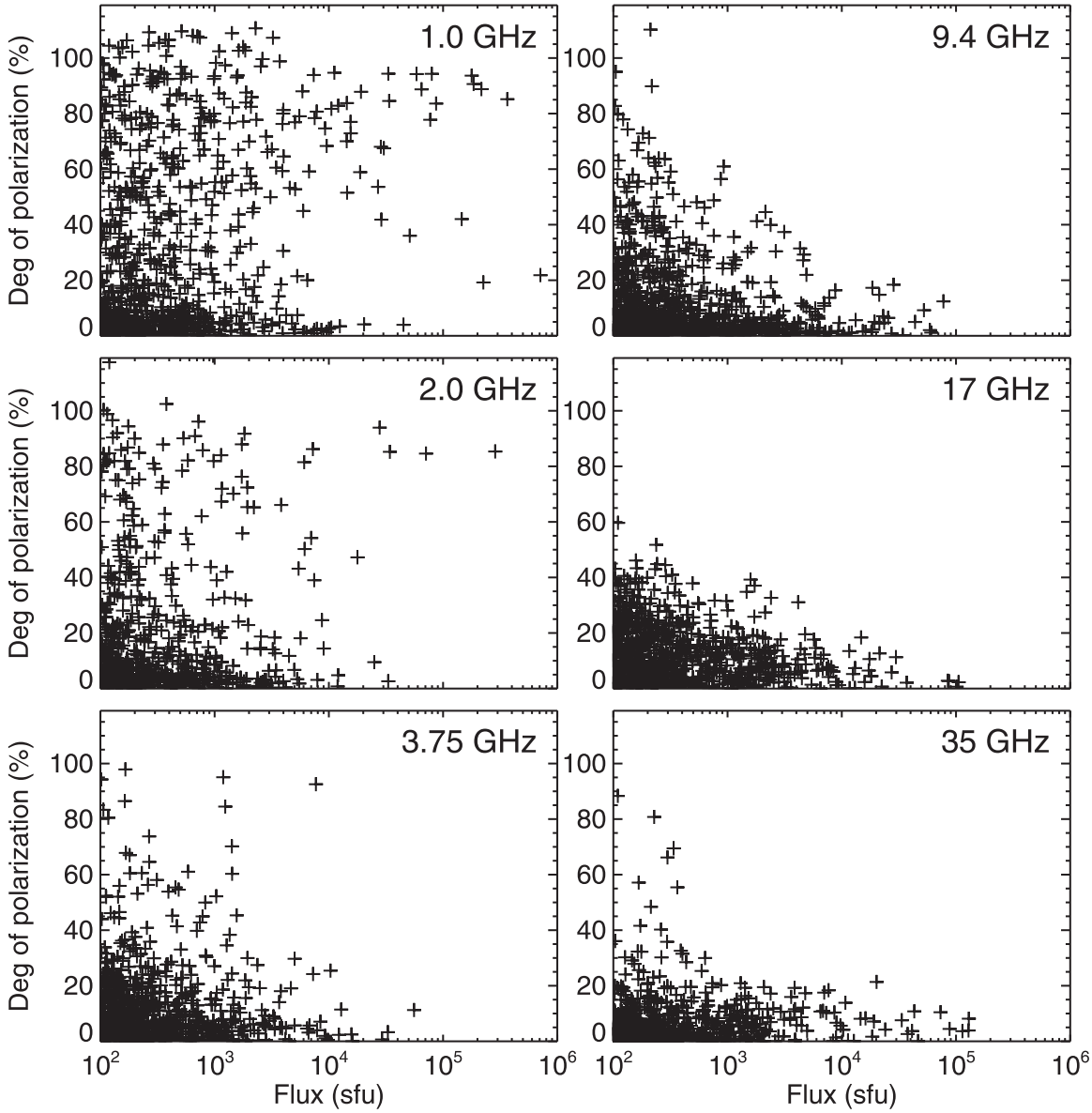

Figure 2. A plot of degree of circular polarization vs. peak flux for NoRP events in excess of 100 sfu. The degree of polarization is calculated at the time of the peak Stokes *I* flux. The numbers of events plotted are 833, 733, 823, 1160, 876, and 1276 at 1.0, 2.0, 3.75, 9.4, 17, and 35 GHz, respectively. At 35 GHz the noise level in the data can be quite high, particularly in poor weather conditions, so we expect that many of the weaker detections there are not reliable.

exceeds 100 sfu. Here, the degree of polarization is measured at the time of peak Stokes *I* flux. Several things are clear from this figure. Of the six frequencies, 1.0 GHz shows the largest number of events with both large flux and a high degree of polarization. 2.0 GHz also exhibits many events with large polarization but generally lower fluxes. The higher frequencies generally have low polarization in all high-flux events: This is not surprising for gyrosynchotron emission, since high fluxes will often be from an optically thick source, thus having a lower polarization. Calculations also show that the degree of polarization of optically thin gyrosynchrotron emission decreases as the frequency increases (e.g., Dulk & Marsh 1982), although it can still be rather large in the case of anisotropic angular distributions of nonthermal electrons (see, e.g., Figures 7–9 in Fleishman & Melnikov 2003). High degrees of polarization at low flux levels may indicate high noise levels in *V* that produce unrealistic values.

As mentioned above, both coherent and incoherent emission can contribute at 1.0 and 2.0 GHz, but incoherent gyrosynchrotron emission should in most cases have a clear signature of flux increasing with frequency up to a single spectral peak. The Tsytovich–Razin effect, which suppresses gyrosynchrotron emission at frequencies not far above the plasma frequency, enhances this effect in the low-frequency region of the spectrum (Ramaty 1969). An exception to this picture is for events occurring beyond the visible limb of the Sun. The location of the gyrosynchrotron spectral peak is strongly correlated with the magnetic field strength in the source (Dulk & Marsh 1982), and field strength generally decreases with height above the solar surface (see, e.g., Figure 1 in Fedenev et al. 2023) such that higher-frequency emission from strong fields low down will not be visible in occulted events, shifting the spectral peak to lower frequencies. However, the number of events in which this is likely to be an issue is small, and none of the strong events that we highlight below are in this category.

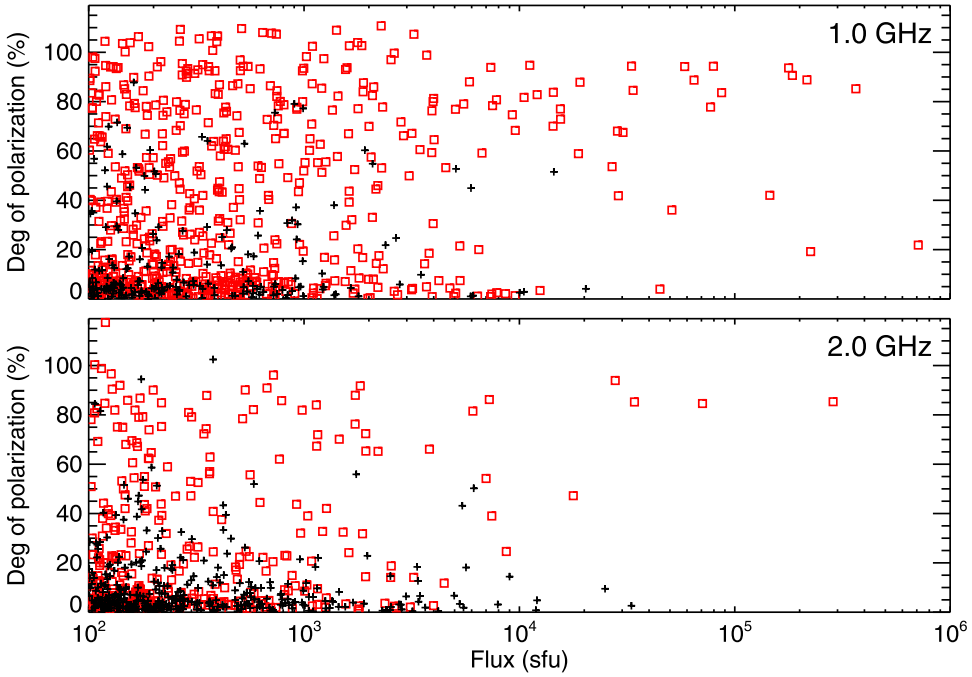

Figure 3. A plot of degree of circular polarization (at the peak of the *I* flux) vs. peak flux for NoRP events in excess of 100 sfu at 1.0 and 2.0 GHz. Events are labeled according to whether the flux at the frequency plotted is greater than (red open squares) or less than (black plus symbols) the corresponding peak flux at 3.75 GHz. A standard solar radio burst gyrosynchrotron spectrum would generally have flux increasing from 1.0 to 2.0 to 3.75 GHz, and thus be among the black symbols.

Thus, we identify bursts in which the 1.0 GHz flux is larger than the 3.75 GHz flux as candidate ECM events.

Figure 3 repeats the plots of Figure 2 for 1.0 and 2.0 GHz, but now separates events in which the spectrum increases with frequency from 1.0 to 2.0 to 3.75 GHz (black plus symbols) from those in which the spectrum decreases with frequency (red open squares). It is striking that most of the high-polarization, high-flux events at 1.0 GHz have decreasing spectra, and thus are unlikely to be gyrosynchrotron emission. At 1.0 GHz, 628 events above 100 sfu have a larger flux at 1.0 GHz than at 3.75 GHz, with 205 having lower flux at 1.0 GHz. Thus, fully three-quarters of the >100 sfu events at 1.0 GHz can be ECM emission. Visual inspection of the NoRP lightcurves for these events confirms that in most cases the 1.0 GHz lightcurve is clearly not compatible with the higher-frequency lightcurves that can be attributed to gyrosynchrotron emission. Three-quarters is a significantly larger fraction than the direct degree of association found by Benz et al. (2005): In a dedicated survey of coherent emission in a sample of 201 flares detected in HXRs by the RHESSI satellite, they found decimeter spikes in only 21 events, or 10% of the sample. In most of those cases the decimetric spikes coincided in time with the peak in HXRs, leading to the inference that they are the coherent emission most closely associated with the main flare energy release (see, e.g., discussion in Battaglia & Benz 2009). However, since we have selected events with 1.0 GHz fluxes greater than 100 sfu, this likely biases the fraction found to have coherent emission. At 2.0 GHz, there are 353 NoRP events over 100 sfu with flux greater than at 3.75 GHz, and 380 events with smaller flux; thus the incidence of dominant coherent emission at 2.0 GHz is significantly smaller than at 1.0 GHz, as inferred previously. Some of the anomalous events in which there is high polarization at 2.0 GHz but less flux than at 3.75 GHz are found to be events in which the 2.0 GHz peak is much larger than the coeval 3.75 GHz flux, but then 3.75 GHz peaks at a very different time; others may be due to radio-frequency interference at either 3.75 GHz or 2.0 GHz (Shimojo & Iwai 2023).

5. The Brightest 1.0 GHz Bursts

Table 1 lists the 23 flares in the NoRP catalog where the 1.0 GHz flux exceeds 10^4 sfu.[18] Here, we have in effect consolidated multiple radio bursts from the NoRP catalog that we believe to be associated with the same flare. A flare from 1991 March 22 has been excluded, since the excess above 10^4 sfu is limited to a single 1 s integration and is likely to be spurious. We note that for a Gaussian source of FWHM of 20″, this flux threshold would require a brightness temperature of 1.6×10^{11} K, so this flux level cannot plausibly be produced by any incoherent emission mechanism, thermal or nonthermal. Plots of the temporal behavior of the NoRP fluxes, the degree of polarization at 1.0, 2.0 and 3.75 GHz, and the corresponding SXR profile are presented in Figure 6 in Appendix A. We omit the flare of 1991 June 6 where the radio flux rises from 1.0 to 3.75 GHz, so there is no evidence for ECM emission in that event.

Many of the flares in Table 1 are large X-class flares with long durations in SXRs, but there are also several M1- or C-class flares (i.e., C flares on the legacy flux scale employed by NOAA at the time of the events), indicating that conditions for production of bright 1.0 GHz emission favor, but do not require, a large flare. The fluxes of the three lower frequencies are plotted on a logarithmic scale in the top panels of Figure 6, and this often obscures just how much brighter the 1.0 GHz emission is compared to 3.75 and/or 2.0 GHz. The fluxes reported in Table 1 demonstrate this: In 16 of the 25 bursts, the 1.0 GHz flux is at least an order of magnitude larger than the

[18] A number of these events were also discussed by Cliver et al. (2011), who also list a sample of bright events in the 1.0–1.6 GHz range.

Table 1
NoRP Solar Radio Bursts Exceeding 10^4 sfu at 1.0 GHz

Date (yy/mm/dd)	SXR Peak Time	SXR[a] Flare	1 GHz Peak Time	1.0 GHz Peak (sfu)	2.0 GHz Peak (sfu)	3.75 GHz Peak (sfu)	1.415 GHz[b] Peak (sfu)	0.61 GHz[b] Peak (sfu)
1989-06-04	02:21:00	M1.4	02:15:02	10515	3594	106	5100	820
1989-08-15	03:17:00	X1.4	03:38:01	28803	11926	16096	77000	28000
1989-11-26	23:53:00	X1.6	00:15:01	15531	673	390	3000	49000
1990-04-15	02:59:00	X2.1	04:40:26	711276	4312	1456	78000	303000
1990-07-30	07:35:00	M6.4	07:59:35	18796	1933	1353	2600	2400
1991-03-23	04:28:00	M9.9	02:41:44	14331	22	20	800	9700
1991-05-16	07:02:00	X1.3	06:58:49	15498	33140	712	94	9700
1991-06-06	01:07:00	X30.2	01:06:18	20332	33106	55690	24000	13000
1991-06-09	01:43:00	X15.1	02:39:09	77220	7252	2485	57000	21000
1991-06-15	08:17:00	X34.7	08:18:14	14447	12064	15771	46000	5000
1991-08-25	01:13:00	X3.0	01:32:25	12470	1931	106	26000	680
2001-04-09	02:56:00	C9.1	02:47:28	86902	965	153	27000	82000
2001-10-19	01:05:00	X2.3	01:24:34	28538	176	1189	8300	32000
2001-11-22	23:30:00	X1.4	22:47:02	12086	841	1181	53000	3500
2002-03-18	02:31:00	M1.4	03:03:19	14373	129	54	27000	2900
2002-04-21	01:51:00	X2.1	02:03:54	145440	8692	1022	>100000	13000
2003-05-28	00:27:00	X5.1	00:27:23	30279	1869	1716	2500	81000
2006-12-13	02:40:00	X4.9	02:28:08	364894	34209	3014	>150000	120000
2011-02-15	01:56:00	X3.1	02:34:17	185170	1457	595	59000	47000
2012-03-05	04:09:00	X1.6	04:28:38	216365	17794	4651	25000	650000
2012-03-07	00:24:00	X7.7	01:07:27	33732	7444	7278	5300	430000
2022-01-29	23:32:00	M1.1	23:30:58	19113	787		9000	
2022-06-13	04:07:00	M3.4	03:53:11	64690	27857	31	98000	3500

Notes.
[a] Flare class is defined on the modern "science-quality" SXR scale. In 1991 and earlier, reported GOES fluxes saturated at X15.7: the three flares from June 1991 were saturated, and the values shown here are from the analysis by Hudson et al. (2024).
[b] From Radio Solar Telescope Network (RSTN, operated by the US Air Force) data. Where two observatories detected the same burst, the larger reported flux was used.

2.0 GHz flux. However, there are a number of bursts where 2.0 GHz is also very bright, implying coherent emission at that frequency also. For reference, we also list the 0.6 and 1.4 GHz fluxes from observations by RSTN. Since the list of bursts was selected based on 1.0 GHz flux, it is not surprising that the 1.4 and 0.6 GHz fluxes are usually smaller than the 1.0 GHz flux, but this is not always the case, and extreme fluxes are often observed at each of these frequencies as well. The log scaling also tends to obscure the degree of variability typical of these bursts; order-of-magnitude variation on timescales of minutes appears to be common.

Of critical interest for understanding this class of bursts is when the bright emission occurs in relation to the impulsive phase, and how long it lasts. As noted above, in the event of 2006 December 6 the brightest emission at 1.4 GHz occurred about an hour after the impulsive phase. Figure 6 shows a range of behavior, but generally the bright emission is long-lasting (several hours in the examples of 1990 April 15, 2002 April 21, 2006 December 13, and 2011 February 15), and can peak over an hour after the SXR peak (e.g., the bursts of 1990 April 15, 1991 March 23, 1991 June 09, and 1991 August 25). It is notable that many of the X-ray flares accompanying the bright 1 GHz emission are long-duration events. We note that Kundu et al. (2004) carried out a detailed study of the 2002 April 21 event: They could not identify EUV signatures corresponding to the bright 1 GHz emission (which they then attributed to plasma emission), but they did find that nonthermal 17 GHz emission and possibly nonthermal HXRs continued during the period of ECM emission.

The frequency extent and time variability of the bright emission can be seen for eight selected events in Figure 4. This shows dynamic spectra from the Hiraiso (1996–2016; see Kondo et al. 1995) and Yamagawa (2016–present; see Iwai et al. 2017) radio spectrographs operated by the National Institute of Information and Communications Technology (NiCT) of Japan. These spectra extend from below 100 MHz to at least 2.0 GHz, and thus cover the frequency range of interest here. Since the data are provided in units of decibels, we do not use these plots for a quantitative discussion, but they do show the extent (in frequency) of bright emission. Consistent with the high 0.6 and 1.4 GHz fluxes in Table 1, these events typically have bright emission over a wide range of frequencies lasting on the order of an hour or more. The bright emission often extends up to 2.0 GHz, but the flux values in Table 1 indicate that it generally does not extend to 3.75 GHz; however, at least for 2006 December 13, Wang et al. (2008) and Tang et al. (2021) report that spikes were seen at that frequency.

Since frequency maps to magnetic field strength for ECM emission, the broadband nature of the bright features in Figure 4 implies that in these very bright bursts the conditions for bright ECM emission typically occur simultaneously over a range of magnetic field strengths, up to a factor of 10. If ECM emission is at the fundamental frequency Ω_B then 2 GHz requires 700 G magnetic fields, while 300 MHz requires 100 G fields. This wide range of field strengths seems to imply that a large volume of the corona is subject to maser action simultaneously. For ECM emission the condition $f_p < \Omega_B$ must then be satisfied throughout the entire volume, which

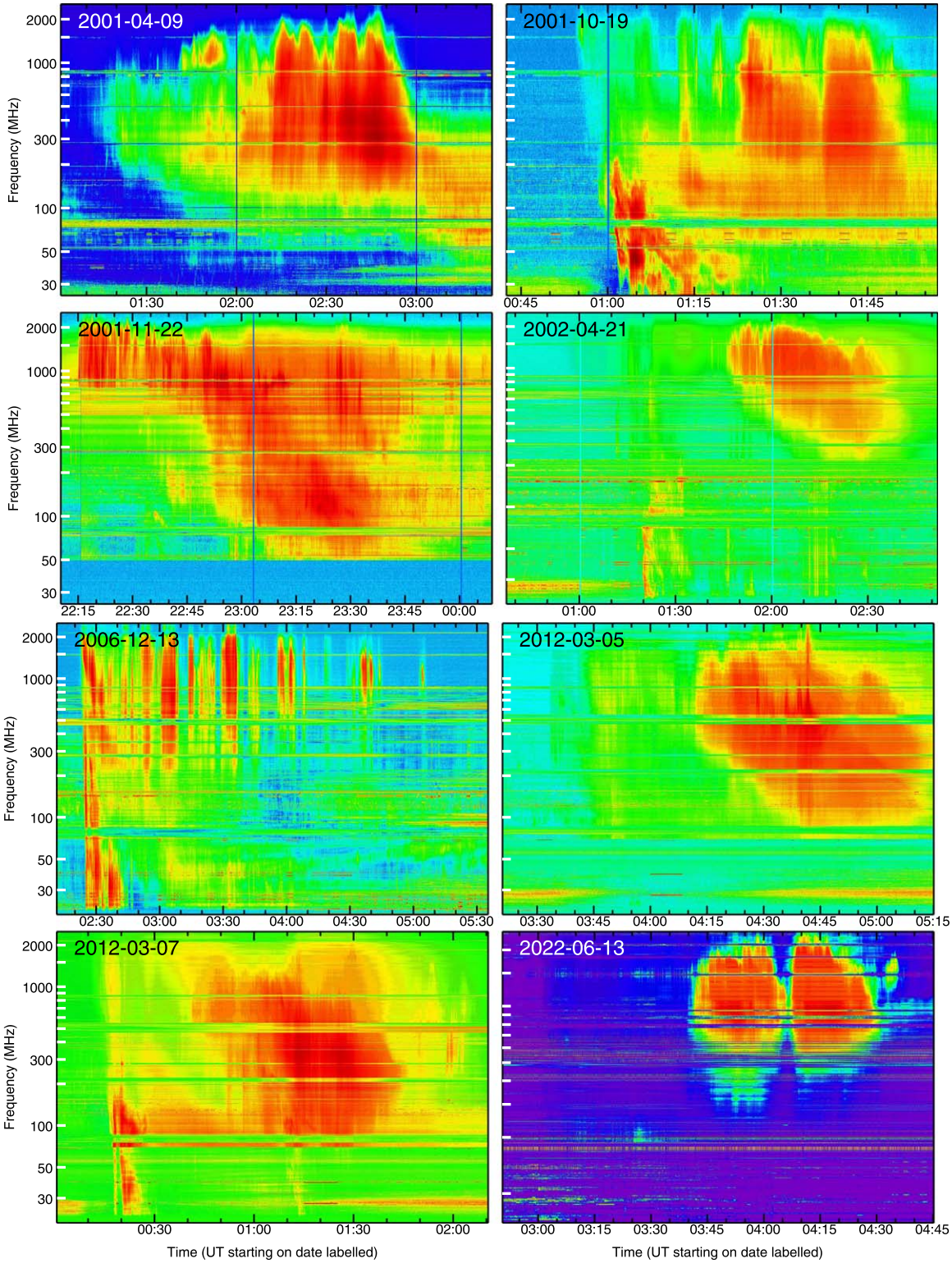

Figure 4. Dynamic spectra of selected bright bursts from the Hiraiso and Yamagawa radio spectrographs operated by NiCT (see text). The plotted time ranges generally match the corresponding plots in Figure 6. The data files are provided in units of decibels. In the color table used, blue is the weakest emission, green is intermediate, and red is the brightest.

seems to argue against an association with the dense postflare loops generally seen in the decay phase of long-duration flares. Cliver et al. (2011) argued that there could still be locations within the loop system where electric fields are present and simultaneously accelerate electrons while evacuating ducts, as they are believed to do in AKR source regions. Melrose & Wheatland (2016) also investigated this scenario and concluded that horseshoe-driven ECM was possible, albeit for spike bursts occurring in conjunction with HXRs. Note that White et al. (1983) show that maser-favoring velocity distributions resembling a "horseshoe" would arise naturally in solar coronal loops following a sudden localized injection of accelerated particles.

The electric fields that accelerate particles in AKR source regions are confined to vertically very narrow "double" layers, of order 10 Debye lengths across, with kilovolt potential drops; in solar postflare loops the Debye length is typically less than 1 mm, tiny compared to the typical length scales of the loops, so it seems unlikely that such small structures could accelerate enough electrons to explain the bright solar bursts. Thus, a direct analogy with the generation of AKR is probably not appropriate for the large bursts discussed here. Since relatively few postflare loop systems produce such bright ECM emission, additional conditions must be required (a conclusion also reached by Cliver et al. 2022). The event of 2006 December 13 has repeated pulses of very bright emission occurring over several hours, suggesting that conditions for bright emission can somehow form, decay, and reform well after the main energy release in the impulsive phase of the flare is long over.

A significant feature of Figure 4 is the morphological similarity of the bright features in the dynamic spectra of all these events. We do not have millisecond-resolution observations of spikes in all these events, but we know that 2006 December 6 and 13 were dominated by spikes: The similarity of the spectral features argues that the other bright bursts were likely also dominated by spikes.

Another important property is polarization. The degree of polarization at the three lower frequencies is plotted in the middle panels for each event in Figure 6. Consistent with the results shown in Figure 2, the polarization is typically high, but rarely at 100%. The highest degrees of polarization seem to occur when the flux is highest (e.g., 1990 July 30, 1991 June 9, 2001 April 9, 2001 October 19, 2006 December 13, and 2012 March 7). Guedel & Zlobec (1991) studied the polarization of solar radio spike bursts and found a wide spread in the degree of polarization, with an apparent center-to-limb variation such that polarization was highest near disk center. Although the two bursts in our sample that have consistently lower polarization (1991 June 15 and 1991 August 25) are both limb events, there are other limb events (e.g., 2002 April 21) with high degrees of polarization, and within a given event the degree of polarization can vary greatly. If ECM is intrinsically 100% polarized, this would imply that either the polarization has been affected by propagation effects or else a significant component of the coherent emission in the NoRP data is not due to ECM.

An interesting feature of Figure 4 is the absence of bright low-frequency emission in the range traditionally associated with plasma emission (below 300 MHz) at the times when the 1.0 GHz emission is brightest. Low-frequency radio bursts can be seen in the impulsive phase in several of the events in Figure 4 (notably 2001 October 19, 2002 April 21, 2006 December 13, and 2012 March 7), but there is no such emission later when the 1.0 GHz emission is bright. The absence of emission such as Type III bursts from electron beams on open field lines, and the clear lower-frequency bound to the frequency range of bright emission in most events, suggests that the conditions for the bright ECM emission are confined to regions of closed magnetic field.

6. Extreme Flux Limits

An issue of some importance is the question of just how bright ECM bursts can be in this frequency range. This is relevant for benchmarking the impacts of space weather (e.g., Operations, Research, and Mitigation Subcommittee 2018; Institute for Defense Analyses 2019). Riley (2012) and Riley & Love (2017) describe an approach for estimating the probability of event occurrence exceeding a specific threshold given a power-law distribution of fluxes.

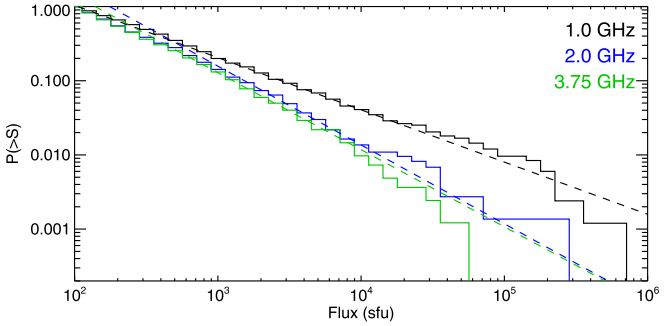

Figure 5. Cumulative probability distributions for the NoRP peak flux at 1.0 (black), 2.0 (blue), and 3.75 (green) GHz, for bursts larger than 100 sfu. The corresponding dashed lines are power-law fits to the 1000–10,000 sfu range.

Those papers note the value of using cumulative distributions for analysis, i.e., distributions representing the number of events observed above a given flux value. Figure 5 plots the cumulative probability distributions of fluxes above 100 sfu from the NoRP burst catalog at 1.0, 2.0, and 3.75 GHZ, together with power-law fits derived from the range 10^3–10^4 sfu. A single power law (index –0.70, fitted from 132 events lying between 10^3 and 10^4 sfu) fits the 1.0 GHz cumulative distribution across most of the range from 100 to 10^5 sfu, with an excess above the fit at around 10^5 sfu. As noted above, an individual flare may be represented by multiple entries in the NoRP catalog, particularly at 1.0 GHz, and this factor may contribute to the excess at $\sim 10^5$ sfu. The fits at 2.0 and 3.75 GHz are similar to each other and somewhat steeper than the 1.0 GHz distribution (power-law indices -1.06 and -1.04 from 94 and 100 events, respectively), but they are above the actual distributions at lower flux levels, indicating that a single power law is not appropriate across the entire range of fluxes. It is possible that the 1.0 GHz fluxes are dominated by ECM events down to 100 sfu, whereas the lower-flux regime at 2.0 and 3.75 GHz has a larger fraction of gyrosynchrotron events contributing with a different distribution. The 2.0 GHz distribution stays close to the power-law fit out to 2×10^5 sfu, while the 3.75 GHz distribution drops below the power law at fluxes beyond 10^4 sfu. The formal uncertainties in the power-law index fits are of order 10%. The power-law indices for the cumulative distributions correspond to power laws of -1.70, -2.06, and -2.04 for the flux occurrence distribution functions above 100 sfu. Nita et al. (2002) fitted power laws to 40 yr of radio bursts above 100 sfu at various frequencies, and found occurrence distribution function indices of -1.83 for both 1.0–1.7 GHz and 2.0–3.8 GHz ranges. Giersch et al. (2017) analyzed the distributions of bursts in the RSTN data (which, they note, suffer from reporting issues that produce undersampling), and, fitting over the full range of fluxes above 100 sfu, they found power-law indices of -1.88, -1.82, and -2.01 at 0.6, 1.4, and 2.7 GHz, respectively. The differences in power-law fits between the different surveys can be attributed at least in part to the different flux ranges being used for the fits.

If we assume that the fitted power laws continue to apply beyond the fitted flux range, we can apply the formalism of Riley (2012) to estimate the incidence of high fluxes. We assume an average coverage of 10 hr day^{-1} for the NoRP observations from 1988 to 2023 (36 yr) that were used to derive

the radio burst catalog; scaling this to 100 yr of 24 hr coverage yields a factor of 6.67. We find that we would expect to see nine bursts over 10^6 sfu at 1.0 GHz in 100 yr, 1.4 at 2.0 GHz, and 0.5 at 3.75 GHz. At the probability level of 50%, the largest bursts that might be seen in 100 yr are 5×10^7 sfu at 1.0 GHz, 3×10^6 sfu at 2.0 GHz, and 1×10^6 sfu at 3.75 GHz.

However, if the distributions do not follow the power-law fits beyond 10^6 sfu, then these numbers will be overestimates. Hudson et al. (2024) provide an extensive discussion of fitting the rollover of the flare SXR flux distribution at high flux levels, but that rollover is much more pronounced than those in Figure 5, and we do not attempt such a fit for the radio flux distributions. The nature of Figure 1 suggests that individual maser spikes saturate after a few milliseconds but that conditions for maser action can reestablish somewhere else in the emitting volume quickly. There may be limitations on this process that could affect the upper limit to fluxes, e.g., if the formation of a maser in a certain region limits the simultaneous or subsequent formation of maser action within a volume around that location, possibly because of the effect of the maser radiation on the velocity distribution in the volume that it irradiates. Better theoretical understanding of the mechanism of these bursts is required to further address the question of practical upper limits to extreme fluxes. Note that Giersch et al. (2017) carried out an extreme-event analysis based on their fits to the RSTN burst data, and estimated an upper limit to the extreme flux at 1.4 GHz of 3.2×10^6 sfu over a 100 yr period.

7. Summary

In this paper, we investigate the incidence of ECM emission in solar radio bursts. We use a revised catalog of radio bursts observed by the NoRP from 1988 to 2023, consisting of 3800+ radio bursts, and focus primarily on the 1.0 GHz data since previous work has suggested that ECM emission can be prominent there. We can distinguish coherent emission at 1 GHz from incoherent gyrosynchrotron emission based on the radio spectrum: Gyrosynchrotron emission at 1 GHz usually has a spectrum rising with frequency, so bursts in which 1 GHz is stronger than higher-frequency measurements are unlikely to be incoherent gyrosynchrotron. Based on this criterion, three-quarters of all bursts exceeding 100 sfu at 1 GHz and half of the bursts at 2 GHz have a significant coherent emission component, assumed to be ECM. The advantage of NoRP data is that the degree of circular polarization in the radio burst is also measured: The catalog shows that most very bright bursts at 1 GHz are highly polarized, consistent with a coherent emission mechanism. The brightest emission seems to be most highly polarized, but it does not appear that the coherent emission is always 100% polarized.

As suggested by the study of the famous 2006 December 6 burst, the brightest 1 GHz emission tends to occur well after the impulsive phase of the flare, and can last for an hour or more. This implies that the source of the energetic electrons that radiate the brightest 1 GHz bursts is not the main energy release in the flare: These radio bursts are apparently fundamentally different from the better-studied spikes in the impulsive phase of flares, which are often associated with the electrons that produce flare HXR emission (e.g., Güdel et al. 1991; Benz et al. 2005; Battaglia & Benz 2009) and/or microwave emission (Fleishman et al. 2003). A pronounced characteristic of the very bright bursts is that they extend across a surprisingly wide frequency range for quite a long period, dynamic spectra show the structure associated with ECM often extending down at least to 300 MHz and up to 2.0 GHz, but not often beyond 2.0 GHz. The corresponding range of coronal magnetic field strengths (assuming radio emission at $f = \Omega_B$) is 100–700 G—why ECM should favor this range of field strengths is a question needing further study. Note that the delay in the bright ECM emission means that there is little connection to the gyrosynchrotron emission produced by a flare, thus ruling out application of the model invoked by Fleishman & Mel'nikov (1998) to explain spikes during the impulsive phase.

Six events in the NoRP catalog have 1.0 GHz fluxes exceeding 10^5 sfu. The distribution of peak fluxes at 1.0 GHz over the period of the NoRP burst catalog obeys a power law out to about 10^6 sfu. This can be extrapolated to an estimate of the largest solar radio burst that can be expected; in a 100 yr period, at 1.0 GHz this could be as high as 5×10^7 sfu. A flux at this level extending from 0.3 to 2 GHz would have severe impacts on cell-phone reception and global navigation systems across most of the sunlit hemisphere of the Earth. However, this estimate relies on the power law continuing to larger fluxes; if there is a saturation effect that truncates the flux distribution, then the upper limit will not be this high. Similarly, peak fluxes as high as 3×10^6 and 1×10^6 sfu could be expected at 2.0 and 3.75 GHz, respectively.

It is worth noting that a 10^6 sfu radio burst on a star 10 pc distant would produce 2.3 mJy of radio flux at Earth, which is easily detectable by modern radio telescopes. Thus, the brighter solar ECM bursts would be readily detectable if occurring on nearby stars, and indeed there have been high-sensitivity observations suggesting analogs of spike bursts on dMe stars (e.g., Abada-Simon et al. 1997; Zhang et al. 2023). By analogy with terrestrial AKR and Jovian DAM, ECM is also the favored explanation for the coherent rotationally modulated radio bursts observed in brown dwarf and magnetic B stars which are believed to have magnetic field structures dominated by a dipole component, much like planetary magnetospheres. Then an important question is whether ECM from solar flares is relevant for such systems where the ECM is not necessarily associated with flares. AKR exhibits a lot of fine structure, usually with pronounced frequency drift (e.g., Benson et al. 1988; Yearby & Pickett 2022; Taubenschuss et al. 2023, and references therein) that is attributed to motion of the source region up or down magnetic field lines with particularly low plasma density (hence $f_p < \Omega_B$) in the auroral regions of the Earth's magnetosphere. Electric fields play a major role in both accelerating electrons into maser-favoring "horseshoe" velocity distributions and evacuating the field lines (Ergun et al. 2000), and in turn the auroral electric fields are affected by the impact of the solar wind on the magnetosphere. Jovian DAM displays a wide range of fine structure, some associated with the motion across the magnetosphere of the flux tube attached to the Io satellite, and others associated with solar wind parameters (e.g., Ryabov et al. 1997; Clarke et al. 2014; Panchenko et al. 2018). Dynamic spectra of those emissions do not generally look like Figure 1. Solar spike bursts can occur in chains that drift in frequency, but individual decimetric spikes are narrow band (bandwidth of order a few percent at most; e.g., Guedel & Benz 1990; Csillaghy & Benz 1993; Rozhansky et al. 2008; Nita et al. 2008; Dąbrowski et al. 2011; Nita et al. 2014), which is consistent with theoretical consideration of ECM

(Fleishman 2004a, 2004b; Rozhansky et al. 2008). But in solar bursts any drift in frequency is very limited, unlike AKR where drifts of 10% or more in frequency are common in discrete features. Thus, the relationship between the brightest solar ECM bursts and planetary/brown dwarf radio emission is not clear, and requires further investigation.

Acknowledgments

S.W. thanks AFOSR for support for basic research through LRIR 23RVCOR003. The views expressed herein are those of the authors and do not reflect official guidance of the US Government or Dept. of Defense. The appearance of external hyperlinks does not constitute endorsement by the US Dept. of Defense of the contents of such links. D.G. and G.F. acknowledge support from NSF grants AGS-2130832 and AGS-2121632 and NASA grant No. 80NSSC23K0090 to the New Jersey Institute of Technology.

Facility: NoRP.

Data Availability

NoRP data are available publicly from the NAOJ website at http://solar.nro.nao.ac.jp/norp/index.html. The catalog of NoRP solar radio bursts used for this study is available on Zenodo at doi:10.5281/zenodo.10719814. Data from the Hiraiso and Yamagawa radio spectrographs are publicly available at https://solobs.nict.go.jp/radio/cgi-bin/MainDisplay.pl.

Appendix
Event Plots

The following figures (Figure 6) show the temporal behavior of the radio emission in the 1.0 GHz bright events listed in Table 1. In each case the upper panel shows the 1.0, 2.0, and 3.75 GHz data on a logarithmic plot; the middle panel shows the corresponding (absolute) degree of circular polarization of those three frequencies; and the bottom plot shows the 3.75, 9.4, 17, and 35 GHz data on a linear scale, for comparison, along with the time profile of the GOES SXR emission from the associated flare. Note that the radio emission in the bottom panel is generally believed to be gyrosynchrotron emission from nonthermal electrons accelerated in the flare in the impulsive phase, with possible contributions from thermal bremsstrahlung emission in the decay phase. The emission at 1 GHz, and occasionally that at 2.0 and 3.75, requires brightness temperatures in excess of 10^{11} K for any plausible source size, which requires a coherent emission.

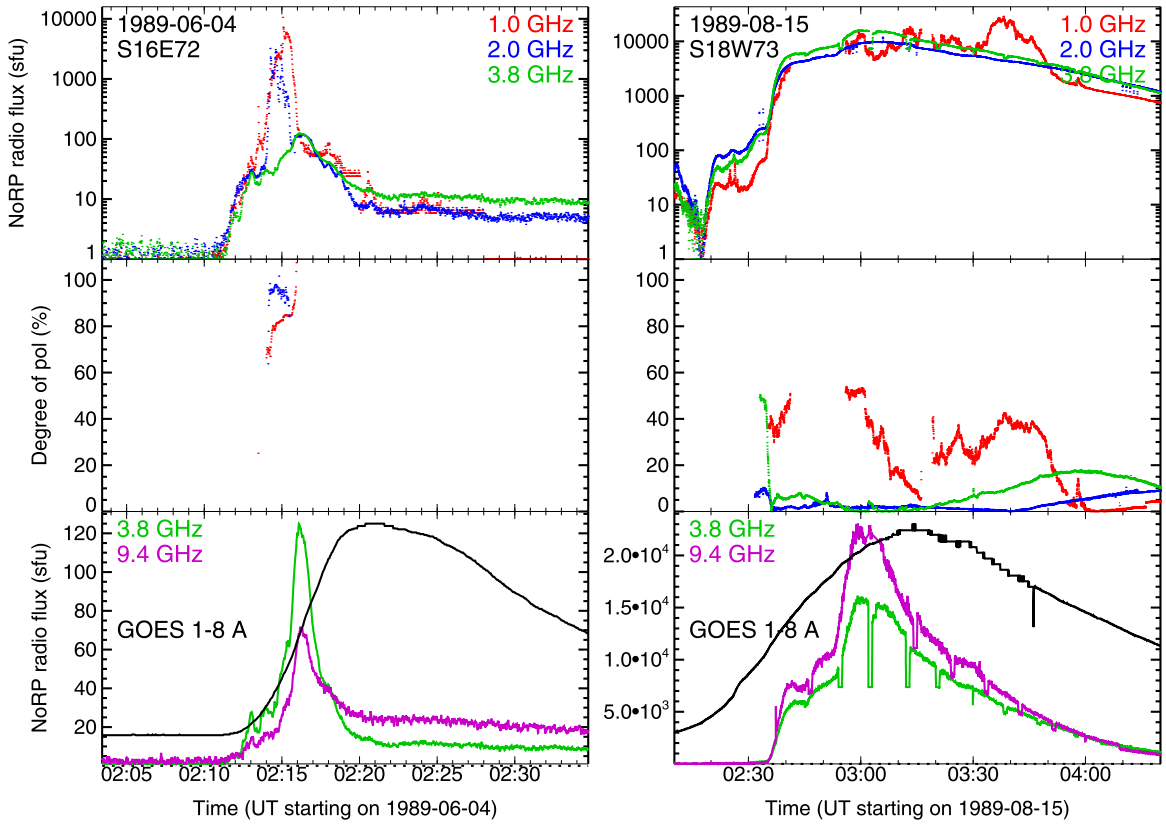

Figure 6. Temporal behavior of the flares listed in Table 1. The upper panel in each case shows the 1.0 (red), 2.0 (blue), and 3.75 GHz (green) data on a logarithmic plot; the middle panel shows the corresponding (absolute) degree of circular polarization of those three frequencies at flux levels above 200 sfu; and the bottom plot shows the 3.75 (green), 9.4 (purple), 17 (orange), and 35 GHz (gray) data on a linear scale, for comparison, along with the time profile of the GOES SXR emission (black line) from the associated flare. The flare date and location (to within about 10 heliographic degrees) are shown in the upper left of each set of panels.

(The complete figure set (11 images) is available.)

ORCID iDs

Stephen M. White https://orcid.org/0000-0002-8574-8629
Masumi Shimojo https://orcid.org/0000-0002-2350-3749
Kazumasa Iwai https://orcid.org/0000-0002-2464-5212
Timothy S. Bastian https://orcid.org/0000-0002-0713-0604
Gregory D. Fleishman https://orcid.org/0000-0001-5557-2100
Dale E. Gary https://orcid.org/0000-0003-2520-8396
Jasmina Magdalenic https://orcid.org/0000-0003-1169-3722
Angelos Vourlidas https://orcid.org/0000-0002-8164-5948

References

Abada-Simon, M., Lecacheux, A., Aubier, M., & Bookbinder, J. A. 1997, A&A, 321, 841
Battaglia, M., & Benz, A. O. 2009, A&A, 499, L33
Benson, R. F., Mellott, M. M., Huff, R. L., & Gurnett, D. A. 1988, JGRA, 93, 7515
Benz, A. O. 1986, SoPh, 104, 99
Benz, A. O., Grigis, P. C., Csillaghy, A., & Saint-Hilaire, P. 2005, SoPh, 226, 121
Benz, A. O., Guedel, M., Isliker, H., Miszkowicz, S., & Stehling, W. 1991, SoPh, 133, 385
Benz, A. O., Su, H., Magun, A., & Stehling, W. 1992, A&AS, 93, 539
Carrano, C. S., Bridgwood, C. T., & Groves, K. M. 2009, RaSc, 44, RS0A25
Cerruti, A. P., Kintner, P. M., Gary, D. E., et al. 2008, SpWea, 6, 10
Chernov, G. P. 2011, Fine Structure of Solar Radio Bursts (Berlin: Springer)
Clarke, T. E., Higgins, C. A., Skarda, J., et al. 2014, JGRA, 119, 9508
Cliver, E. W., Schrijver, C. J., Shibata, K., & Usoskin, I. G. 2022, LRSP, 19, 2
Cliver, E. W., White, S. M., & Balasubramaniam, K. S. 2011, ApJ, 743, 145
Csillaghy, A., & Benz, A. O. 1993, A&A, 274, 487
Dąbrowski, B. P., Rudawy, P., & Karlický, M. 2011, SoPh, 273, 377
Dröge, F. 1977, A&A, 57, 285
Dulk, G. A., & Marsh, K. A. 1982, ApJ, 259, 350
Ergun, R. E., Carlson, C. W., McFadden, J. P., et al. 2000, ApJ, 538, 456
Fedenev, V. V., Anfinogentov, S. A., & Fleishman, G. D. 2023, ApJ, 943, 160
Fleishman, G. D. 2004a, AstL, 30, 603
Fleishman, G. D. 2004b, ApJ, 601, 559
Fleishman, G. D., Gary, D. E., & Nita, G. M. 2003, ApJ, 593, 571
Fleishman, G. D., & Mel'nikov, V. F. 1998, PhyU, 41, 1157
Fleishman, G. D., & Melnikov, V. F. 2003, ApJ, 587, 823
Gary, D. E. 2019, arXiv:1901.09262
Gary, D. E., & Bastian, T. S. 2021, in Space Weather Effects and Applications, ed. A. J. Coster et al. (New York: Wiley), 141
Gary, D. E., & Keller, C. U. 2004, Solar and Space Weather Radiophysics—Current Status and Future Developments (Dordrecht: Kluwer)
Giersch, O. D., Kennewell, J., & Lynch, M. 2017, SpWea, 15, 1511
Güdel, M., Aschwanden, M., & Benz, A. O. 1991, A&A, 251, 285
Guedel, M., & Benz, A. O. 1990, A&A, 231, 202
Guedel, M., & Zlobec, P. 1991, A&A, 245, 299
Hallinan, G., Antonova, A., Doyle, J. G., et al. 2006, ApJ, 653, 690
Hewitt, R. G., Melrose, D. B., & Ronnmark, K. G. 1982, AuJPh, 35, 447
Holman, G. D., Eichler, D., & Kundu, M. R. 1980, in IAU Symp. 86, Radio Physics of the Sun, ed. M. R. Kundu & T. E. Gergely (Dordrecht: Reidel), 457
Hudson, H. S., Cliver, E. W., White, S. M., et al. 2024, SoPh,, 299, 39
Institute for Defense Analyses 2019, Space Weather Benchmarks, Vol. Group Report 10982 (IDA Science and Technology Policy Institute)
Iwai, K., Kubo, Y., Ishibashi, H., et al. 2017, EP&S, 69, 95
Kondo, T., Isobe, T., Watari, S., & Tokumaru, M. 1995, J. Commun. Res. Lab., 42, 111
Kundu, M. R., Garaimov, V. I., White, S. M., & Krucker, S. 2004, ApJ, 600, 1052
Lee, L. C., Kan, J. R., & Wu, C. S. 1980, P&SS, 28, 703
Liu, Z., Gary, D. E., Nita, G. M., White, S. M., & Hurford, G. J. 2007, PASP, 119, 303
Lysenko, A. L., White, S. M., Zhdanov, D. A., et al. 2023, ApJ, 954, 122
McLean, D. J., & Labrum, N. R. 1985, Solar Radiophysics (Cambridge: Cambridge Univ. Press)
Melrose, D. B. 1976, ApJ, 207, 651
Melrose, D. B., & Dulk, G. A. 1982, ApJ, 259, 844
Melrose, D. B., Rönnmark, K. G., & Hewitt, R. G. 1982, JGRA, 87, 5140
Melrose, D. B., & Wheatland, M. S. 2016, SoPh, 291, 3637
Nakajima, H., Sekiguchi, H., Sawa, M., et al. 1985, PASJ, 37, 163
Nita, G. M., Fleishman, G. D., & Gary, D. E. 2008, ApJ, 689, 545
Nita, G. M., Fleishman, G. D., Gary, D. E., Marin, W., & Boone, K. 2014, ApJ, 789, 152
Nita, G. M., Gary, D. E., Lanzerotti, L. J., & Thomson, D. J. 2002, ApJ, 570, 423
Nita, G. M., Gary, D. E., & Lee, J. 2004, ApJ, 605, 528
Panchenko, M., Rošker, S., Rucker, H. O., et al. 2018, A&A, 610, A69
Ramaty, R. 1969, ApJ, 158, 753
Riley, P. 2012, SpWea, 1, 02012
Riley, P., & Love, J. J. 2017, SpWea, 15, 53
Rozhansky, I. V., Fleishman, G. D., & Huang, G.-L. 2008, ApJ, 681, 1688
Ryabov, B. P., Zarka, P., Rucker, H. O., Ryabov, V. B., & Boudjada, M. Y. 1997, in Proc. of Int. Workshop 4, Planetary Radio Emission IV, ed. H. O. Rucker, S. J. Bauer, & A. Lecacheux (Vienna: Austrian Academy of Science Press), 65
Shimojo, M., & Iwai, K. 2023, GSDJ, 10, 114
Slottje, C. 1978, Natur, 275, 520
Song, Q., Huang, G., & Tan, B. 2012, ApJ, 750, 160
Operations, Research, and Mitigation Subcommittee 2018, Space Weather Phase 1 Benchmarks (National Science and Technology Council), https://www.sworm.gov/publications/2018/Space-Weather-Phase-1-Benchmarks-Report.pdf
Takakura, T., & Scalise, E. 1970, SoPh, 11, 434
Tang, J.-F., Wu, D.-J., Wan, J.-L., Chen, L., & Tan, C.-M. 2021, RAA, 21, 148
Taubenschuss, U., Fischer, G., Pisa, D., Santolík, O., & Soucek, J. 2023, in Planetary, Solar and Heliospheric Radio Emissions IX, ed. C. K. Louis et al., 103089
Trigilio, C., Leto, P., Leone, F., Umana, G., & Buemi, C. 2000, A&A, 362, 281
Wang, S. J., Yan, Y. H., Liu, Y. Y., et al. 2008, SoPh, 253, 133
White, S. M., & Franciosini, E. 1995, ApJ, 444, 342
White, S. M., Melrose, D. B., & Dulk, G. A. 1983, PASA, 5, 188
Wu, C. S., & Lee, L. C. 1979, ApJ, 230, 621
Yearby, K. H., & Pickett, J. S. 2022, JGRA, 127, e2021JA029499
Zhang, J., Tian, H., Zarka, P., et al. 2023, ApJ, 953, 65